ASTRO-H

INSTRUMENT CALIBRATION REPORT
ON-AXIS TELESCOPE EFFECTIVE AREA
ASTH-TEL-CALDB-TELAREA

Version 1.2

December 22, 2016

ISAS/ GSFC

Prepared by: Tahir Yaqoob and GSFC Hitomi Science Data Center

Table of Contents

Introduction 4
1.1 Purpose 4
1.2 Scientific Impact 4
2 Release CALDB 20161122 4
2.1 Updates 5
3 Release CALDB 20160624 6
3.1 Data Description 6
3.2 Data Analysis 7
3.3 Results 7
3.4 Final Remarks 10

CHANGE RECORD PAGE (1 of 2)

DOCUMENT TITLE: On-axis Telescope Effective Area			
ISSUE	DATE	PAGES AFFECTED	DESCRIPTION
Version 1.0	June 2016	All	Caldb release 20160624
Version 1.1	Aug 2016	Section 3.2	Add clarification on number of photons used to create these files.
Version 1.1	Dec 2016	8-10	Caldb release 20161222

Introduction

1.1 Purpose

This document describes data in the CALDB files containing the on-axis effective area (derived from raytracing simulations), as a function of energy for each of the four X-ray telescopes aboard Hitomi (SXT-S for SXS, SXT-I for SXI, HXT-1 for HXI1, and HXT-2 for HXI2). In addition, for HXT-1 and HXT-2, an image for each telescope describes the shadowing effect of the HXI baffle. There is one CALDB file for each telescope.

1.2 Scientific Impact

The on-axis effective area data for SXT-S and SXT-I are used by the tasks *ahsxtarfgen* (for SXT-S and SXT-I) and *hxirspeffimg* (for HXT-1 and HXT-2) in the calculation of the combined telescope and detector effective area (ARF) for arbitrary off-axis angles and arbitrary energies. There are two effective area functions in each CALDB file (i.e. two functions for each telescope). One of the functions is based on a coarse energy grid, whilst the other is based on a finer energy grid that captures all of the necessary atomic features at an energy resolution that is better than the instrument that the CALDB file is associated with. Raytracing simulations show that the ratio of the off-axis effective area to the on-axis effective area is only a weak function of energy. Since the on-axis high-resolution effective area captures the strong energy dependence of the reflectivity and transmission, the run-time for calculating the off-axis effective area at sufficiently high energy resolution can be significantly reduced, by more than an order of magnitude. This is achieved in the tasks *ahsxtarfgen* and *hxirspeffimg* by (1) running the raytracing code xrtraytrace on a coarse energy grid, (2) modeling the ratio of the resulting effective area to the on-axis coarse effective area in the CALDB file, (3) evaluating the fitted function on the fine energy grid, and then (4) using the fine-grid on-axis effective area in the CALDB file to arrive at the fine-grid off-axis effective area.

The baffle shadowing data in the primary extensions of the HXI CALDB files are used by the task *hxirspeffimg* for calculating a flat-field efficiency map or exposure image.

2 Release CALDB 20161122

Filename	Valid data	Release date	CALDB Vrs	Comments
ah_sxi_telarea_20140101v002.fits	2014-01-01	20161122	V005	
ah_hx1_telarea_20140101v002.fits	2014-01-01	20161122	V005	
ah_hx2_telarea_20140101v002.fits	2014-01-01	20161122	V005	

2.1 Updates

The on-axis telescope effective area files for SXI, HXI1, and HXI2 have significantly better statistical errors than the corresponding files in the previous release. The file were made by running the raytracing code xrtraytrace with 10,000,000 photons per energy, 100 times greater than for the previous runs. The new telescope effective areas as a function of energy are shown below.

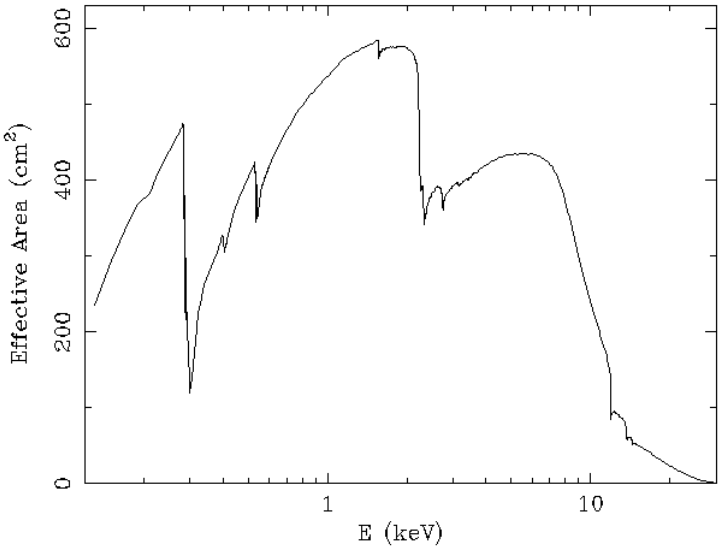

On-axis SXI effective area as function of fine-grid energy in the EFFAREAFNE extension of the SXI CALDB file.

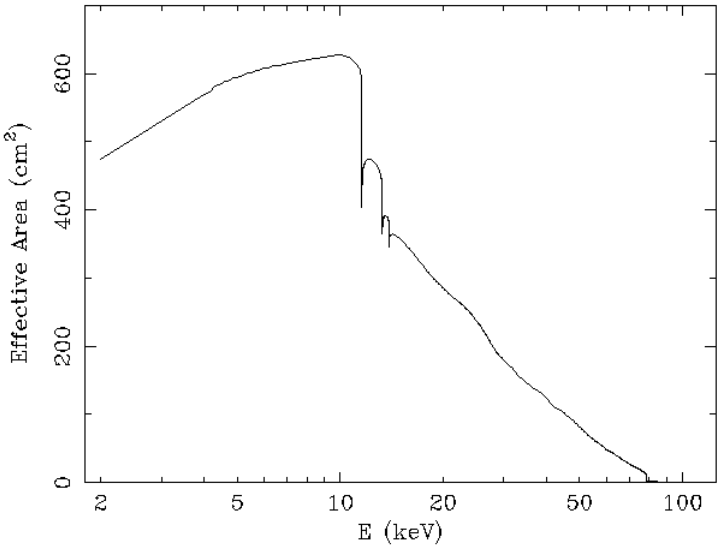

On-axis HXI1 telescope effective area as function of fine-grid energy in the EFFAREAFNE extension of the HXI1 CALDB file.

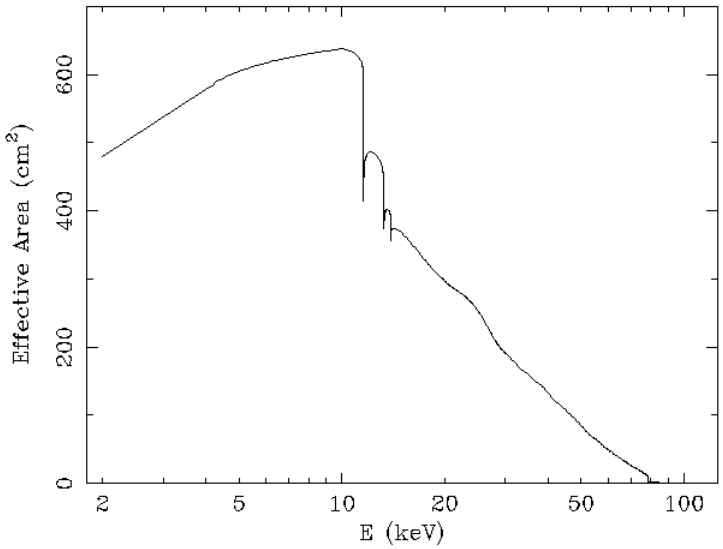

On-axis HXI2 telescope (HXT-2) effective area as function of fine-grid energy in the EFFAREAFNE extension of the HXI2 CALDB file.

3 Release CALDB 20160624

Filename	Valid data	Release date	CALDB Vrs	Comments
ah_sxs_telarea_20140101v003.fits	2014-01-01	2016-06-24	V004	
ah_sxi_telarea_20140101v001.fits	2014-01-01	2016-06-24	V004	
ah_hx1_telarea_20140101v001.fits	2014-01-01	2016-06-24	V004	
ah_hx2_telarea_20140101v001.fits	2014-01-01	2016-06-24	V004	

3.1 Data Description

The data in the CALDB files is as follows:

Extension	Instruments	Content
PRIMARY	SXS, SXI	Blank
PRIMARY	HXI	Baffle shadowing image
EFFAREAFNE	SXS, SXI, HXI	Effective area vs. energy, fine grid
EFFAREACRS	SXS, SXI, HXI	Effective area vs. energy, coarse grid

The HXI baffle images are images of the detectors in RAWX and RAWY coordinates, with each pixel value lying between 0.0 and 1.0. The pixel value represents the ratio of the number of photons at the focal plane with the baffle in place, to the number that would reach that pixel on the focal plane if there were no baffle. Thus, the images represent an effective efficiency due to the baffle

The on-axis effective area data cover the energy range 0.030 to 30.000 keV for SXT-S (991 points) and SXT-I (811 points), for the fine-grid effective area. The coarse-grid effective area is a subset of 36 of these points, covering the same energy band. For HXT-1 and HXT-2 the fine grid has 975 points in the 2-120 keV energy range and the coarse grid is a subset of 280 of these energy points covering the same bandpass.

3.2 Data Analysis

A simplified model of the HXI baffle is applied to photons raytraced through the HXT-1 and HXT-2 telescopes. The raytraced photons are generated by the task *xrtraytrace,* using an incident uniform flat photon distribution, in the 4-70 keV range, in order to map the radial intensity reduction due to the baffle. A 128x128 RAWX, RAWY image made from these photons is compared with an image made from the same raytracing runs without the baffle in place.

The HXI and SXI on-axis effective area curves are generated with xrtraytrace using the fine energy grids described above, injecting 100,000 photons per energy. For the SXS the file is generated using 10000000 photons per energy. The CALDB files used for the raytracing run are those included in the 160624 CALDB release. The events file output from each raytrace run contains information about all of the photons that impact the focal plane. Selecting those events that include a double reflection (one reflection on a primary mirror, and one on a secondary mirror), and comparing with the injected number of photons at each energy enables computation of the effective area as a function of energy. The value of the geometric area used is equal to the value of the keyword GEOMAREA in the CALDB Telescope Description File (TDF) for each telescope.

3.3 Results

It was found that the raytraced images for HXT-1 and HXT-2 with and without the HXI baffle were statistically consistent with every detector pixel having an efficiency of 1.0 (see Fig. 1). This is consistent with the fact that the projected size of the baffle aperture at the focal plane is larger than the HXI detector. Therefore, the current baffle shadowing maps for HXI1 and HXI2 have uniform values of 1.0 for every RAWX and RAWY pixel.

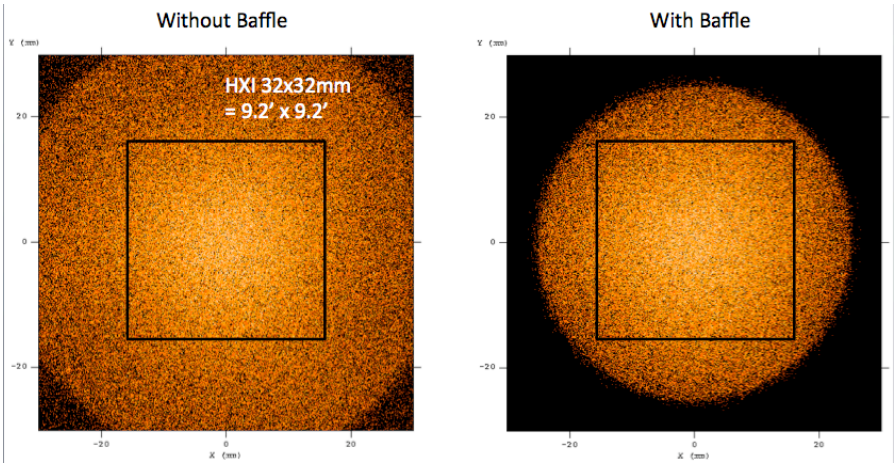

Figure 1: Raytracing image for HXI1 with a uniform illumination without the baffle (left) and with the baffle (right). The black square represents the HXI detector region. The ratio of the two images inside the black square is consistent with a uniform value of 1.0 across the region.

The on-axis effective area on the fine energy grids are illustrated in Figs. 2-5 for the four telescopes, as labelled.

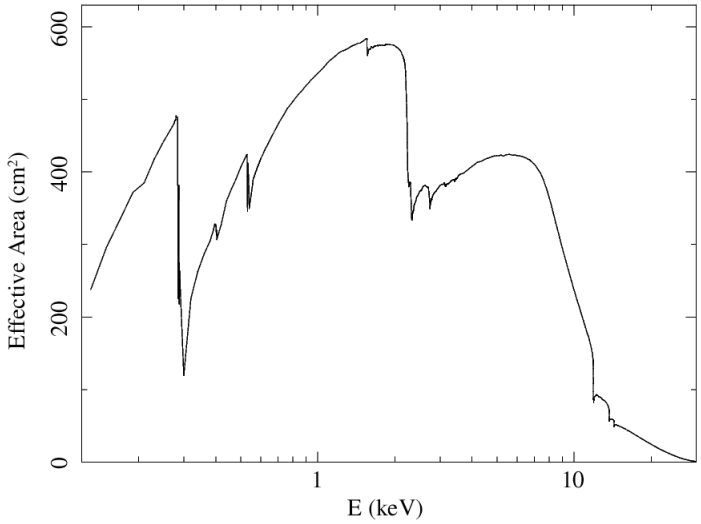

Figure 2: On-axis SXS effective area as function of fine-grid energy in the EFFAREAFNE extension of the SXS CALDB file.

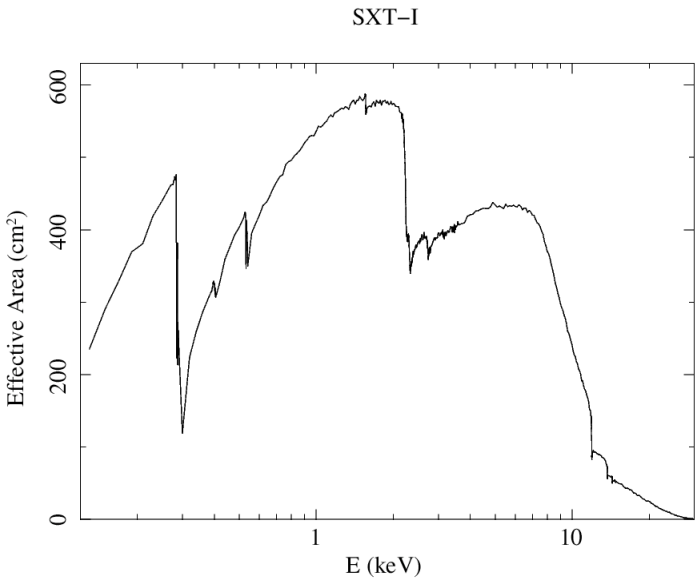

Figure 3: On-axis SXI effective area as function of fine-grid energy in the EFFAREAFNE extension of the SXI CALDB file.

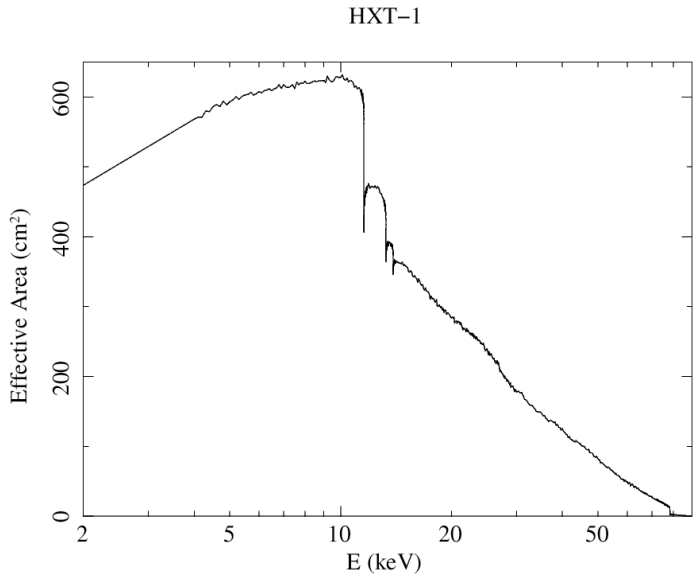

Figure 4: On-axis HXI1 telescope effective area as function of fine-grid energy in the EFFAREAFNE extension of the HXI1 CALDB file.

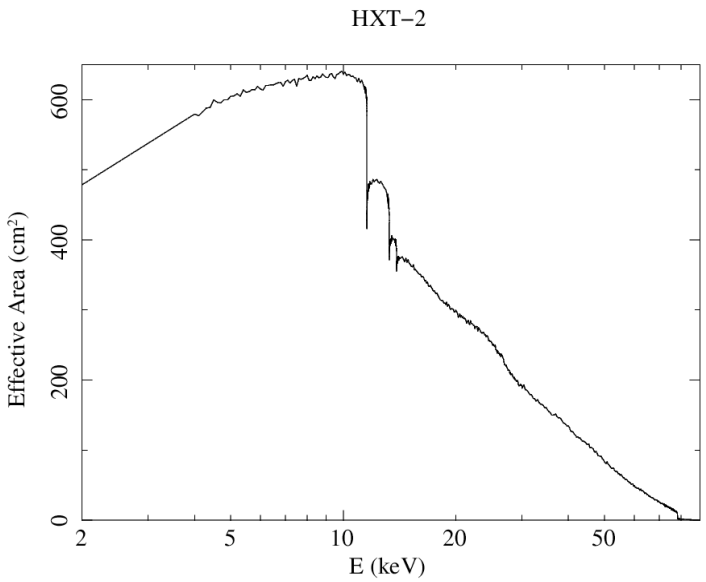

Figure 5: On-axis HXI2 telescope (HXT-2) effective area as function of fine-grid energy in the EFFAREAFNE extension of the HXI2 CALDB file.

3.4 Final Remarks

This is the second official release of this document. The changes affect the ARF/RSP for SXI, HXI1, and HXI2.